



**HAL**  
open science

## Microtubule polymerization state and clathrin-dependent internalization regulate dynamics of cardiac potassium channel Microtubule and clathrin control of K V 1.5 channel

Dario Melgari, Camille Barbier, Gilles Dilanian, Catherine Rücker-Martin, Nicolas Doisne, Alain Coulombe, Stéphane N Hatem, Elise Balse

### ► To cite this version:

Dario Melgari, Camille Barbier, Gilles Dilanian, Catherine Rücker-Martin, Nicolas Doisne, et al.. Microtubule polymerization state and clathrin-dependent internalization regulate dynamics of cardiac potassium channel Microtubule and clathrin control of K V 1.5 channel. *Journal of Molecular and Cellular Cardiology*, 2020, 144, pp.127-139. 10.1016/j.yjmcc.2020.05.004 . hal-02945112

**HAL Id: hal-02945112**

**<https://hal.sorbonne-universite.fr/hal-02945112>**

Submitted on 22 Sep 2020

**HAL** is a multi-disciplinary open access archive for the deposit and dissemination of scientific research documents, whether they are published or not. The documents may come from teaching and research institutions in France or abroad, or from public or private research centers.

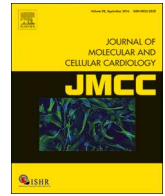
L'archive ouverte pluridisciplinaire **HAL**, est destinée au dépôt et à la diffusion de documents scientifiques de niveau recherche, publiés ou non, émanant des établissements d'enseignement et de recherche français ou étrangers, des laboratoires publics ou privés.



ELSEVIER

Contents lists available at ScienceDirect

## Journal of Molecular and Cellular Cardiology

journal homepage: [www.elsevier.com/locate/yjmcc](http://www.elsevier.com/locate/yjmcc)

# Microtubule polymerization state and clathrin-dependent internalization regulate dynamics of cardiac potassium channel

## Microtubule and clathrin control of $K_V1.5$ channel

Dario Melgari<sup>a</sup>, Camille Barbier<sup>a</sup>, Gilles Dilanian<sup>a</sup>, Catherine Rücker-Martin<sup>c</sup>, Nicolas Doisne<sup>a</sup>, Alain Coulombe<sup>a</sup>, Stéphane N. Hatem<sup>a,b</sup>, Elise Balse<sup>a,\*</sup>

<sup>a</sup> INSERM UMRS1166, ICAN - Institute of CardioMetabolism and Nutrition, Sorbonne Université, Paris, France

<sup>b</sup> Institut de Cardiologie, Hôpital Pitié-Salpêtrière, Paris, France

<sup>c</sup> INSERM U999, University of Paris-Sud, Centre Chirurgical Marie Lannelongue, France

## ARTICLE INFO

## Keywords:

Atrial myocytes  
Potassium channel dynamics  
Clathrin  
Cytoskeleton  
Atrial remodeling

## ABSTRACT

Ion channel trafficking powerfully influences cardiac electrical activity as it regulates the number of available channels at the plasma membrane. Studies have largely focused on identifying the molecular determinants of the trafficking of the atria-specific  $K_V1.5$  channel, the molecular basis of the ultra-rapid delayed rectifier current  $I_{Kur}$ . Besides, regulated  $K_V1.5$  channel recycling upon changes in homeostatic state and mechanical constraints in native cardiomyocytes has been well documented. Here, using cutting-edge imaging in live myocytes, we investigated the dynamics of this channel in the plasma membrane. We demonstrate that the clathrin pathway is a major regulator of the functional expression of  $K_V1.5$  channels in atrial myocytes, with the microtubule network as the prominent organizer of  $K_V1.5$  transport within the membrane. Both clathrin blockade and microtubule disruption result in channel clusterization with reduced membrane mobility and internalization, whereas disassembly of the actin cytoskeleton does not. Mobile  $K_V1.5$  channels are associated with the microtubule plus-end tracking protein EB1 whereas static  $K_V1.5$  clusters are associated with stable acetylated microtubules. In human biopsies from patients in atrial fibrillation associated with atrial remodeling, drastic modifications in the trafficking balance occurs together with alteration in microtubule polymerization state resulting in modest reduced endocytosis and increased recycling. Consequently, hallmark of atrial  $K_V1.5$  dynamics within the membrane is clathrin- and microtubule- dependent. During atrial remodeling, predominance of anterograde trafficking activity over retrograde trafficking could result in accumulation of  $K_V1.5$  channels in the plasma membrane.

## 1. Introduction

The current understanding of basic cardiac electrophysiology has undergone a profound transformation. The classical theory that the cardiac action potential is generated by the successive opening or closing of different ion channels with distinct biophysical properties is now challenged by accumulating evidence indicating that these proteins belong to a large molecular network undergoing continuous dynamic regulation. Thus, functional ion channel expression results from highly-integrated cellular activities including post-translational regulation, trafficking, and cell microarchitecture organization.

The pathophysiology of cardiac arrhythmias has begun to be revisited in the light of this new paradigm. A first clue was the discovery of mutations in the *HERG* gene producing a trafficking-defective

channel, and reduced corresponding  $I_{Kr}$  current amplitude, in inherited long-QT syndrome [1]. Another example is the observation that hypokalemia, a risk factor for cardiac arrhythmias, reduces hERG channel density at the plasma membrane by promoting channel internalization [2]. We previously reported that  $K_V1.5$  channels, the molecular basis of the atria-specific ultra-rapid delayed rectifier current  $I_{Kur}$ , are stored in submembrane recycling endosomes and are ready for recruitment upon changes in membrane cholesterol content [3] or upon shear stress [4]. The latter process requires activation of the integrin/phosphorylated FAK signaling pathway which becomes constitutively stimulated during atrial dilation as a result of excessive atrial wall cardiac myocyte shear stress, thereby contributing to action potential shortening and increased susceptibility to atrial arrhythmias.

The aim of the present study was to further decipher the trajectory

\* Corresponding author at: INSERM UMRS1166, Faculté de Médecine Pitié-Salpêtrière, 91, Boulevard de l'Hôpital, 75013 Paris, France.

E-mail address: [elise.balse@upmc.fr](mailto:elise.balse@upmc.fr) (E. Balse).

<https://doi.org/10.1016/j.yjmcc.2020.05.004>

Received 14 April 2020; Received in revised form 8 May 2020; Accepted 9 May 2020

Available online 20 May 2020

0022-2828/ © 2020 The Author(s). Published by Elsevier Ltd. This is an open access article under the CC BY-NC-ND license

(<http://creativecommons.org/licenses/by-nc-nd/4.0/>).

and trafficking pathways of  $K_V1.5$  channels and the contribution of these processes to potassium current properties in atrial cardiomyocytes. Specifically, we investigated the role of the cytoskeleton and internalization routes involved in functional  $K_V1.5$  channel expression. There is currently limited information about  $K_V1.5$  channel internalization, reported to be regulated by both dynamin- and dynein-dependent pathways in heterologous expression systems [5,6]. It has been suggested that  $K_V1.5$  internalization could occur *via* caveolae association [7,8], however the clathrin pathway has not yet been directly investigated. Using whole-cell patch-clamp, biochemistry techniques, and cutting-edge imaging approaches, we showed that  $K_V1.5$  channels are highly mobile in the sarcolemma and follow the microtubule network, whereas clathrin pathway is involved as the principal internalization route. In remodeled atrial myocardium from patients in atrial fibrillation (AF), we provide evidence for reduced endocytosis and altered recycling that could contribute to the accumulation of  $K_V1.5$  channels in the sarcolemma of atrial myocytes during disease.

## 2. Results

### 2.1. $K_V1.5$ channels are associated with clathrin vesicles but not with caveolae

The association of  $K_V1.5$  channels with canonical endocytosis pathways was investigated in freshly isolated atrial myocytes (Fig. 1A). Colocalization analysis revealed that  $K_V1.5$  channels co-localized poorly with caveolin-3 (R: 0.08) but associated with clathrin vesicles (R: 0.53) labelled with clathrin light chain (CLC) antibody (Fig. 1A, C)

( $n = 5$  cells, 15 lines/cell). Immunofluorescence images showed that clathrin vesicles were located at the intercalated disc (ID), the lateral membrane (LM), and at the perinuclear level (Figs. S1A, S2B).  $K_V1.5$  and CLC-positives vesicles were located both at the ID and at the LM (Fig. 1C). Electron microscopy revealed the presence of clathrin coated vesicles (CCVs) and clathrin buds at the ID and at the LM (Fig. S1B). Interestingly, CCVs were also observable along the z-lines in atrial sections (Fig. S1B). Quantification showed that the ID displayed an equal amount of buds and internalized vesicles (CCVs) whereas the number of internalized vesicles was superior to the number of buds at the LM, suggesting that the LM is a more active endocytosis zone (Fig. S1D). Immunostaining experiments were also performed in cultured atrial myocytes in which the human  $K_V1.5$  channel fused to the GFP protein (h- $K_V1.5$ -GFP) was overexpressed using an adenoviral vector. In overexpression condition as well, the association of  $K_V1.5$  was observed only with clathrin vesicles (Fig. 1B, D). These observations show that clathrin-dependent endocytosis is likely to be the internalization pathway of  $K_V1.5$  channels in atrial myocytes.

### 2.2. Clathrin pathway regulates the density of functional $K_V1.5$ channels in atrial myocytes

Biotinylation experiments were performed to quantify the abundance of h- $K_V1.5$ -GFP channels on the membrane surface after blockade of the clathrin pathway with sucrose (225 mmol/L) treatment for 2 h. Sucrose prevents clathrin from interacting with the adaptor protein complex AP2 and triggers abnormal formation of microcages [9]. The h- $K_V1.5$ -GFP band was increased by  $1.47 \pm 0.06$  in the membrane

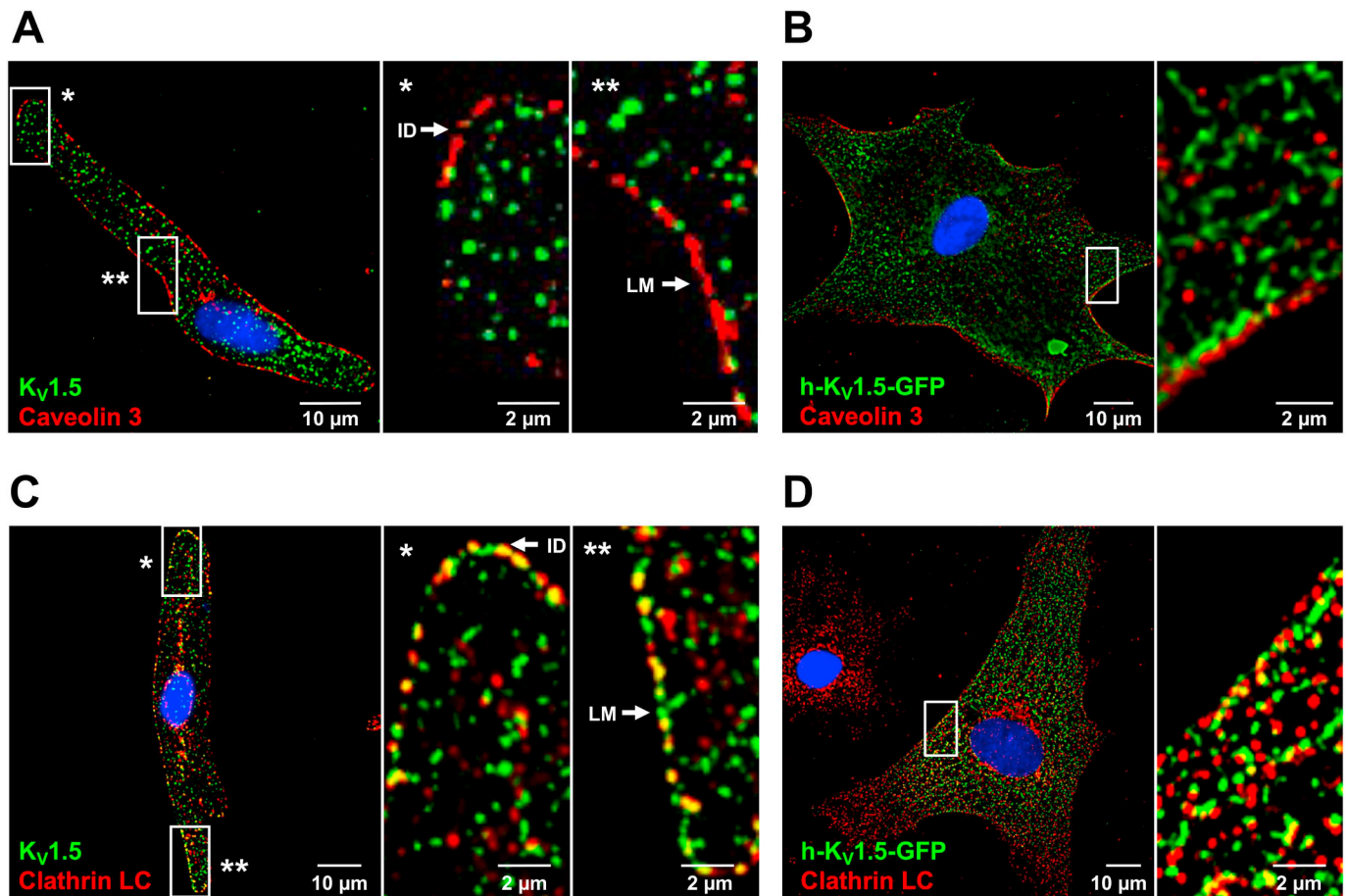


**Fig. 1.**  $K_V1.5$  channels are associated with clathrin vesicles but not with caveolae in atrial myocytes. A, C, Freshly isolated atrial myocytes stained with  $K_V1.5$  and (A) caveolin-3 or (C) clathrin light-chain (LC), and enlargements of regions of interest (ROI\* and ROI\*\*). B, D, Cultured atrial cardiomyocytes expressing h- $K_V1.5$ -GFP and stained with (B) caveolin-3 or (D) clathrin-LC, and enlargement of one ROI. LM: Lateral Membrane; ID: Intercalated Disc.

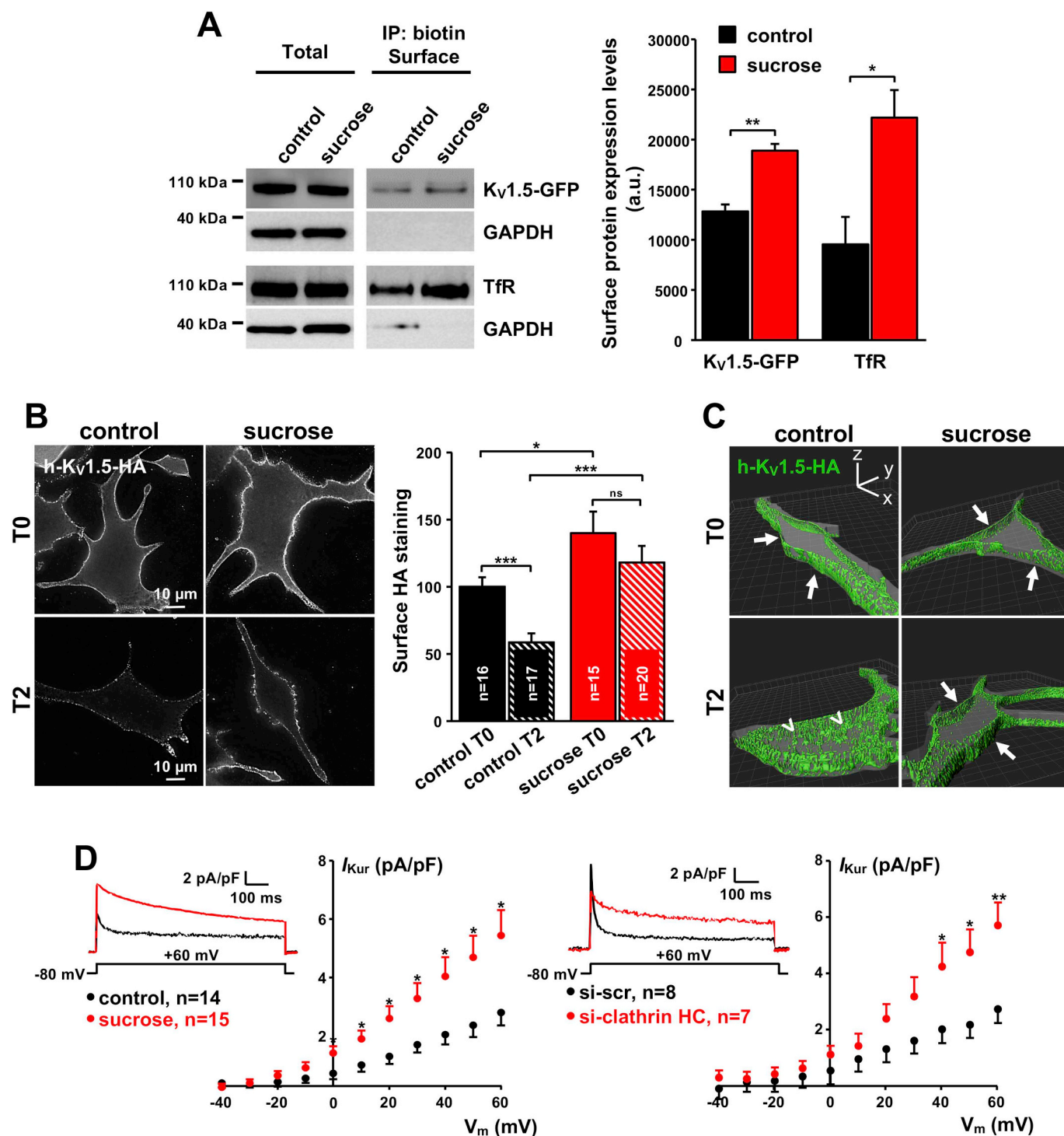


**Fig. 2.** Blockade of clathrin pathway increases abundance of  $K_V1.5$  channels on the membrane surface and corresponding  $I_{Kur}$  current in atrial myocytes. **A**, Representative surface biotinylation assay performed on atrial myocytes expressing h- $K_V1.5$ -GFP (Left) and quantification of surface proteins in control and sucrose conditions (Right). **B**, Surface expression (T0) and internalization of h- $K_V1.5$ -HA channel (T2) in control and sucrose conditions (Left), and summary graphs of the fluorescent HA staining at cell surface at T0 and T2 (Right). **C**, Perspective views of 3D-rendered images (z-projections) at the two time points. Arrows point cell boundaries at T0; arrowheads point channels inside the cell at T2 in control condition. **D**, Current density-voltage relationships of endogenous  $I_{Kur}$  recorded from atrial myocytes in control and sucrose conditions (Left) and transfected with si-scr or si-clathrin heavy-chain (CHC) (Right), and representative traces in the insert \*  $P < .05$ ; \*\*  $P < .01$ ; \*\*\*  $P < .001$ , n = number of cells.

fraction after sucrose treatment (Fig. 2A,  $n = 3$ ). The transferrin receptor was used as a control of clathrin-mediated endocytosis and was increased by  $2.33 \pm 0.21$  in the surface fraction after sucrose treatment (Fig. 2A).

Next, surface fluorescence signal was quantified in cultured atrial

myocytes transfected with h- $K_V1.5$ -HA, the HA tag being located on  $K_V1.5$  extracellular loop. Cells were incubated for 2 h with control medium or sucrose and live stained with anti-HA and secondary Fab A448 antibody before fixation allowing visualization of only pools of channels expressed at the cell surface. Quantification revealed ~40%

increase in  $K_V1.5$  surface staining in sucrose-treated cells at T0 (Fig. 2B). Internalization assay further supported the importance of the clathrin pathway on  $K_V1.5$  channel endocytosis: whereas ~40% of channels were internalized after 2 h (T2) in control condition, internalization was almost completely prevented in sucrose-treated cells (15%, ns from T0) (Fig. 2B). Perspective views of 3D projection of 4  $\mu\text{m}$  stack acquired at 0.2  $\mu\text{m}$  intervals also showed the HA staining at the membrane at T0 and reduced internalization in sucrose-treated cells compared to control at T2 (Fig. 2C).

The effect of clathrin blockade on  $K_V1.5$  anterograde trafficking was also investigated using a trafficking block and release assay [10]. Atrial myocytes overexpressing h- $K_V1.5$ -HA were treated with brefeldin A to prevent ER/Golgi transport and trafficking was restarted for 2 h before addition of sucrose (or control medium). Quantification of surface HA staining (*i.e.* without permeabilization) relative to total HA (*i.e.* after permeabilization) showed that clathrin blockade results in reduced *de novo* delivery of  $K_V1.5$  channel (Fig. S2), as clathrin is also involved in the active transport of cargo proteins at the Golgi exit en route to the plasma membrane [11]. Indeed, immunofluorescence and electron microscopy images showed that clathrin vesicles can be observed in the perinuclear region of freshly isolated cardiomyocytes and surrounding the Golgi apparatus as illustrated by Fig. S2B, C. Then, the endogenous  $K_V1.5$ -mediated current  $I_{Kur}$  was recorded in control and sucrose-treated myocytes by whole-cell patch-clamp. The potassium current density was significantly increased at several tested voltages in sucrose-treated myocytes (Fig. 2D, left). Note that the cell capacitance was not significantly different between control and sucrose-treated cells (control:  $42 \pm 5$  pF, sucrose:  $38 \pm 3$  pF) showing that the surface membrane remains unchanged by the sucrose treatment.  $I_{Kur}$  was also recorded in myocytes in which the clathrin pathway was repressed using a small interfering RNA directed toward the clathrin heavy chain (si-clathrin HC). As observed with sucrose, the  $K_V1.5$ -mediated current was significantly increased at several tested voltages in si-clathrin HC-transfected atrial myocytes (Fig. 2D, right). Note that activation properties of  $I_{Kur}$  were not modified by clathrin blockade (Fig. S3). Despite the fact that clathrin blockade perturbs both anterograde and retrograde trafficking, these results suggest that internalization is the predominantly affected pathway. In fact, this led to an increased amount of  $K_V1.5$  channels on the membrane surface and corresponding  $I_{Kur}$  current. Altogether, these results indicate that clathrin pathway is the major regulator of surface and functional expression of  $K_V1.5$  channels in atrial myocytes.

### 2.3. Clathrin pathway inhibition leads to $K_V1.5$ clusterization and reduced mobility in the sarcolemma of atrial myocytes

Movies of 2 h were acquired from live atrial myocytes upon TIRF illumination to investigate the effect of clathrin blockade on  $K_V1.5$  channels dynamics in the membrane plane. In control condition, h- $K_V1.5$ -GFP channels showed a punctate distribution at the sarcolemma (vesicle mean size:  $0.12 \pm 0.01 \mu\text{m}^2$ ) (Fig. 3A, E) with dynamic movements in the x/y axis (Movie 1A). Upon sucrose treatment, total evanescent field fluorescence (EFF) augmented linearly without reaching a plateau (Fig. 3B) and was increased by ~25% at the end of the movie (Fig. 3C). Note that sucrose did not affect neither cell morphology nor GFP distribution used as control (Fig. S4A, B). Sucrose treatment also led to the accretion of h- $K_V1.5$ -GFP-containing vesicles into large clusters (cluster mean size:  $2.77 \pm 0.05 \mu\text{m}^2$ ) (Fig. 3E, Movie 1B). The number of h- $K_V1.5$ -GFP vesicles having a diameter superior to 0.4  $\mu\text{m}$  started to increase after 30 min of treatment and reached a plateau after 80 min (Fig. 3D). These results suggest that the linear fluorescence increase is likely due to the continuous insertion of vesicles of smaller diameter from submembrane stores. Analysis of two-hour movies acquired from live atrial myocytes in TIRF illumination also revealed that blockade of the clathrin pathway decreased  $K_V1.5$  channels mobility in the x/y axis as illustrated by Fig. 3F, G (Movie 1C).

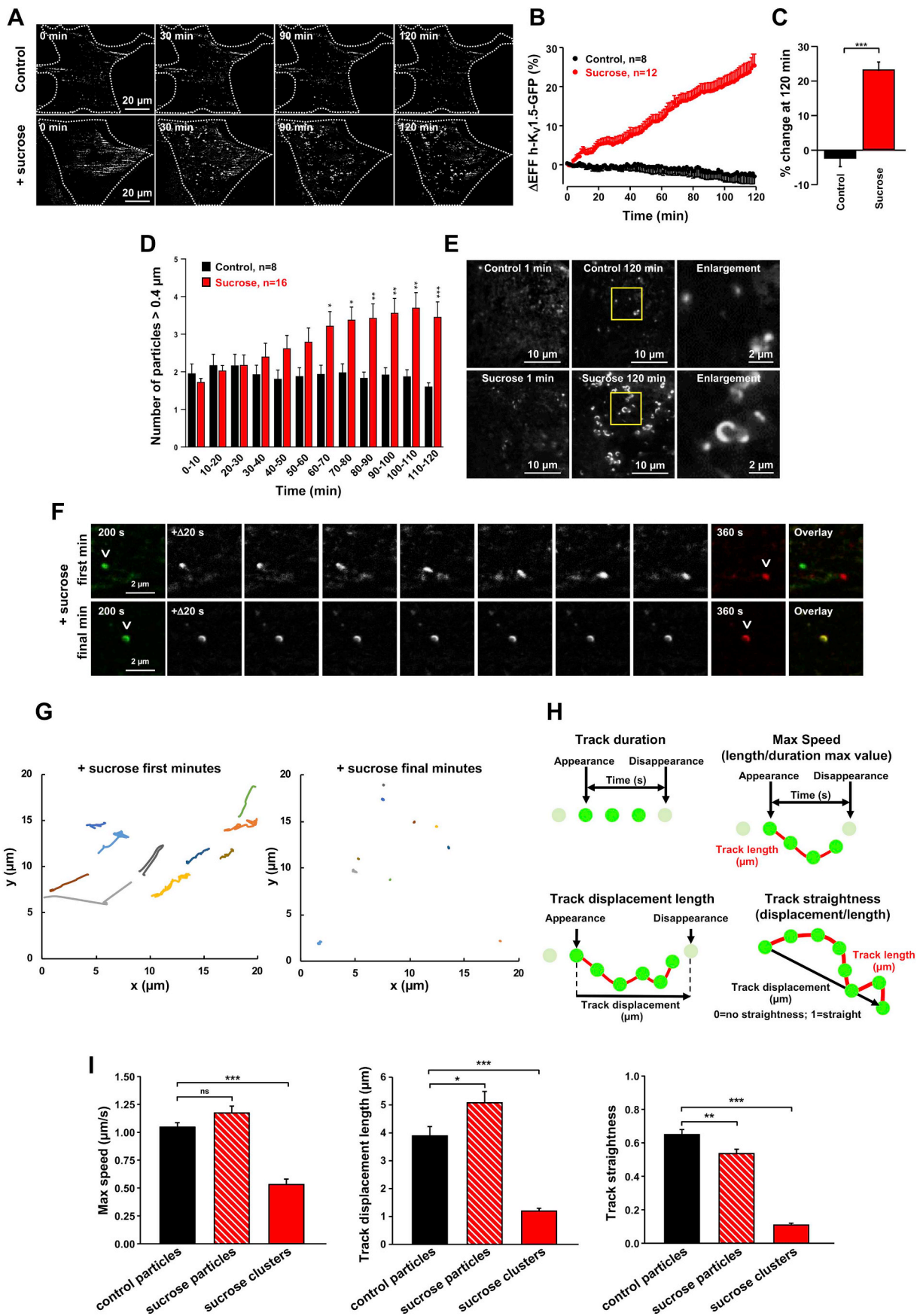
Dynamics of individual h- $K_V1.5$ -GFP vesicles was tracked from 2-min movies in control and sucrose-treated myocytes (Fig. 3D). For the sake of clarity, single particles dynamics refer to track duration, track max speed, track displacement length, and track straightness as illustrated by cartoons in Fig. 3H. In control condition, h- $K_V1.5$ -GFP channels displayed an average run of  $3.89 \pm 0.34 \mu\text{m}$  in the x/y axis, and a mean duration of  $24.5 \pm 3.1$  s. The max speed value was  $1.05 \pm 0.04 \mu\text{m/s}$  (Table S1, Movie 1C). The behavior of h- $K_V1.5$ -GFP vesicles was also analyzed on the basis of the straightness of their tracks, 0 representing disordered runs and 1 representing 100% linear movement. In control condition the average track straightness was  $0.65 \pm 0.03$  (Table S1), suggesting a structured displacement in the membrane plane. Clathrin blockade profoundly reduced h- $K_V1.5$ -GFP mobility in the membrane plane, in particular in large sucrose-induced clusters (Fig. 3D). Large clusters persisted in the membrane plane for almost the whole duration of the recordings ( $100.6 \pm 3.3$  s, Movie 1D), with an average displacement length of  $1.19 \pm 0.1 \mu\text{m}$  and a track straightness of  $0.11 \pm 0.01$ . Track max speed was also deeply affected, with an average value of  $0.53 \pm 0.05 \mu\text{m/s}$  (Table S1). Interestingly, sucrose-mediated clathrin blockade did not completely abolish the presence of moving particles. However, sucrose treatment induced an increased persistence at the membrane plane compared to control: average displacement length  $5.08 \pm 0.41 \mu\text{m}$ , average track duration of  $38.6 \pm 3.4$  s (Table S1). Track straightness was also reduced ( $0.54 \pm 0.03$ ), while track max speed was not significantly affected (Table S1). Overall, this indicates that clathrin blockade reduced h- $K_V1.5$ -GFP mobility by inducing particles clusterization and increasing clusters persistence in the sarcolemma.

### 2.4. Role of the cytoskeleton in $K_V1.5$ mobility in the sarcolemma

As h- $K_V1.5$ -GFP vesicles displayed structured displacements in control atrial myocytes, we investigated the association of the channel with the microtubule network and the actin cytoskeleton.

The effect of cytoskeleton disrupting agents on abundance of h- $K_V1.5$ -GFP channels on the membrane surface was examined using whole-cell patch-clamp and live-cell immunostaining. Disruption of either microtubule with colchicine (2 h, 10  $\mu\text{mol/L}$ ) or actin cytoskeleton with cytochalasin-D (24 h, 10  $\mu\text{mol/L}$ ) had no effect on endogenous  $I_{Kur}$  in atrial myocytes (Fig. S5A, B). Similarly, neither colchicine nor cytochalasin-D significantly modified the total amount of the channel on the membrane surface as quantified in atrial myocytes transduced with an extracellularly-HA-tagged h- $K_V1.5$  channel [12] (Fig. S5C, D). These observations suggest that both anterograde and retrograde trafficking were equally affected by cytoskeleton disrupting agents, and that no changes correspond to an equilibrium between the two opposite processes. Therefore, the effects of cytoskeleton disrupting agents on both anterograde and retrograde trafficking was then further dissected out. Trafficking block and release assay (Fig. S6A) showed that colchicine treatment reduced  $K_V1.5$  abundance on the membrane surface (relative to total  $K_V1.5$ -HA) by ~40% whereas cytochalasin-D reduced anterograde trafficking by ~15%. Internalization assay (Fig. S6B, and perspective views of 3D images Fig. S7) showed that colchicine reduced  $K_V1.5$  endocytosis by ~37% whereas cytochalasin-D reduced internalization by ~18%. These observations support the already demonstrated participation of microtubules and microfilaments in anterograde and retrograde trafficking (for review see [11]).

Atrial myocytes transduced with h- $K_V1.5$ -GFP were labelled with the CellLight® Tubulin-RFP fluorescent dye and imaged by TIRF microscopy using dual color acquisitions. In the sarcolemma, h- $K_V1.5$ -GFP vesicles followed the microtubule network as shown in Fig. 4A. The mobility pattern of h- $K_V1.5$ -GFP vesicles was analyzed using the standard deviation (SD) projection from a time series. The resulting SD map was aligned with the average (fixed) tubulin image.  $K_V1.5$  vesicles exhibited a linear movement that followed the microtubule network (Fig. 4B). TIRF movies were acquired for 2 h from atrial myocytes



(caption on next page)

**Fig. 3.** Blockade of the clathrin pathway induces  $K_v1.5$  clusterization and reduces  $K_v1.5$  channel mobility in the sarcolemma of atrial myocytes. A, TIRF images from 2 h time-lapse movie of cultured atrial myocytes expressing h- $K_v1.5$ -GFP in control (top) or under sucrose (bottom) treatment. B, Mean time courses of total evanescent field fluorescence (EFF) intensity in response to sucrose treatment vs control. C, EFF intensity changes at the end of the movies. D, Number of h- $K_v1.5$  channel vesicles over time in control and sucrose conditions. E, Regions of interest (ROI) from TIRF movies at the beginning and at the end of the recording in control (top) and sucrose (bottom) conditions, and enlargements of outlined regions. F, TIRF images of h- $K_v1.5$ -GFP vesicles displacements during first minutes (top) and final minutes (bottom) of sucrose treatment. Arrowheads point vesicles at the beginning and at the end of 160 s tracking. G, Tracks generated from TIRF movies representing the displacement of h- $K_v1.5$ -GFP channels in the x/y axis during first (left) and final minutes (right) of a 2 h movie. H, Cartoons illustrating parameters measured from fast tracking movies. Green dots represent tracked h- $K_v1.5$ -vesicles (diameter  $\geq 0.4 \mu\text{m}$ ). I, Plots of h- $K_v1.5$ -EGFP channel dynamics in control and sucrose conditions. ns, not significant; \* $P < .05$ ; \*\*\* $P < .001$ ;  $n = 10$ – $15$  cells, 50–100 tracks/cell. (For interpretation of the references to color in this figure legend, the reader is referred to the web version of this article.)

treated with the microtubule disrupting agent colchicine (10  $\mu\text{mol/L}$ ) (Movie 2A). The h- $K_v1.5$ -GFP EFF signal was stable at the beginning, then the number of h- $K_v1.5$ -GFP vesicles ( $> 0.4 \mu\text{m}$ ) in the sarcolemma increased by  $\sim 39\%$  in the sarcolemma after 40 min and reached a maximum increase of  $\sim 74\%$  after 1-h colchicine treatment (Fig. 4C). After 2 h treatment with colchicine, the particles mobility was severely compromised in the x/y axis (Fig. 4D). In addition, 2 min TIRF movies were acquired in order to measure single particles dynamics in control (EtOH) and in the presence of colchicine (Movie 2B). Over a total of 10 acquired movies only 4 moving particles were detected in the presence of colchicine, while 43 moving particles were tracked over 9 movies in control. In addition, the mobility of those few moving particles was strongly affected by the presence of colchicine: track duration was increased to  $24.0 \pm 7.1$  s (vs  $13.4 \pm 1.6$  s in control) and track displacement length was reduced to  $0.99 \pm 0.21 \mu\text{m}$  (vs  $4.17 \pm 0.37 \mu\text{m}$  in control). Track straightness and track max speed were also all significantly decreased (Fig. 4E, Table S1).

Similar experiments were repeated in atrial myocytes transduced with h- $K_v1.5$ -GFP and labelled with the CellLight® Actin-RFP fluorescent dye. As shown in Fig. 5A, h- $K_v1.5$ -GFP vesicles did not track along the actin cytoskeleton in the sarcolemma but rather moved between actin fibers. Examination of the mobility pattern of vesicles related to the actin cytoskeleton using SD projection and averaged (fixed) actin image showed linear movements of h- $K_v1.5$ -GFP particles preferentially outside of microfilament grids (Fig. 5B). After overnight treatment with an inhibitor of actin polymerization, cytochalasin-D (10  $\mu\text{mol/L}$ ), the particles mobility was not massively compromised in the x/y axis (Fig. 5C, Movie 3A). Analysis of 2 min long fast-tracking TIRF movies (Movie 3B) showed that cytochalasin-D did not significantly affect h- $K_v1.5$ -GFP particles dynamics: average track displacement length of  $4.00 \pm 0.41 \mu\text{m}$  vs  $3.24 \pm 0.38 \mu\text{m}$ ; average track duration of  $13.86 \pm 1.49$  s vs  $11.61 \pm 1.57$  s with cytochalasin-D (Fig. 5D, Table S1). Track max speed and track straightness were also unaffected by the treatment with cytochalasin-D. However, the total number of moving particles was reduced by the treatment. A total of 43 particles were tracked over 10 movies in control condition, while, 18 moving particles over 9 acquired movies could be tracked in the presence of cytochalasin-D. These observations might indicate a partial involvement of the actin cytoskeleton in the membrane plane.

Quantifications of h- $K_v1.5$ -GFP vesicles associated with tubulin or with actin in the membrane plane showed that  $K_v1.5$  was twofold more associated with microtubules ( $\sim 36\%$ ) than with actin microfilaments ( $\sim 18\%$ ) in control conditions (Fig. 6A, B). After colchicine treatment, the percentage of h- $K_v1.5$ -GFP associated with microtubule remnants was reduced by half whereas the association of h- $K_v1.5$ -GFP with actin residues was not significantly modified by cytochalasin-D (Fig. 6B). Altogether, these results support the preferential involvement of microtubules over actin in  $K_v1.5$  dynamics in the sarcolemma of atrial myocytes. Finally, large clusters observed after clathrin blockade were positives for tubulin markers: whereas h- $K_v1.5$ -GFP vesicles were associated by  $54.7 \pm 5.9\%$  to dynamic microtubules stained with the plus-end tracking protein EB1 in control condition, sucrose treatment reduced this association to  $26.3 \pm 2.9\%$  (Fig. 6C, D). Conversely, after sucrose treatment, h- $K_v1.5$ -GFP were more associated with acetylated (*i.e.* stables) microtubules ( $43.8 \pm 7\%$ ) compared to control

( $11.4 \pm 2.7\%$ ) (Fig. 6C, D). Thus, after clathrin blockade, h- $K_v1.5$ -GFP clusters are preferentially associated with stable microtubules.

### 2.5. Alteration of trafficking pathways in atrial fibrillation

Finally, we examined  $K_v1.5$  channel trafficking pathways during AF. First, several trafficking-related proteins were quantified using western blot assays performed with total lysate extracted from permanent AF ( $n = 4$ – $5$ ) and control (sinus rhythm, SR,  $n = 5$ ) patients (Fig. 7A, B).  $K_v1.5$  total protein expression level was increased by  $35.2 \pm 7.1\%$  in permanent AF patients compared to SR controls. A marked increase in effectors related to trafficking was observed in AF such as endocytosis markers (clathrin heavy-chain, CHC:  $+49.1 \pm 14.8\%$  and dynamin-2:  $+111.8 \pm 13.3\%$ ), retrograde molecular motors (myosin 6:  $+89.0 \pm 12.8\%$  and dynein:  $+31.2 \pm 9.4\%$ ), proteins associated with early endosomes (EEA1:  $+69.3 \pm 13.9\%$  and Rab5:  $+53.6 \pm 8.4\%$ ), and finally recycling-endosome associated proteins (Rab-4:  $+103.4 \pm 9.1\%$  and Rab11:  $+64.3 \pm 6.1\%$ ). Moreover, while the total expression level of tubulin was not modified in permanent AF, the expression of dynamic microtubules was increased (plus-end tracking protein EB1:  $+37.5 \pm 4.0\%$ ) whereas stable microtubules expression was decreased (acetylated tubulin:  $-40.0 \pm 8.2\%$ ) compared to control.

We then analyzed the distribution of two selected endocytosis markers in the atria of AF patients. Frozen slices from biopsy samples of three AF patients and three SR controls were stained with antibodies against clathrin light-chain (CLC) or dynamin-2. Wheat Germ Agglutinin (WGA) was used in order to stain cardiomyocyte membranes. Series of 8–9 images for each sample were then acquired using high resolution 3-D deconvolution microscopy. The acquired images were then analyzed in Fiji where an algorithm was designed in order to calculate the ratio between “membrane mean intensity” and “total mean intensity” for each selected marker (Fig. 7C, D). Both markers were almost evenly distributed within the control tissue, as the signal mean intensity was just slightly higher in the membrane region (membrane/total ratio  $1.08 \pm 0.02$  and  $1.02 \pm 0.01$  for CLC and dynamin-2 respectively). Interestingly, in AF condition a small but significant  $\sim 10\%$  decrease in the membrane/total ratio was observed for both CLC and dynamin-2 ( $0.98 \pm 0.02$  and  $0.92 \pm 0.01$  respectively). Considering the increase in total protein level for clathrin, this decrease might suggest a reduced clathrin-mediated internalization.

Altogether, these results indicate that the trafficking machinery is globally altered in patients with permanent AF.

## 3. Discussion

The present study unravels the mechanisms behind the high mobility of  $K_v1.5$  channels trafficking within and from the sarcolemma of atrial cardiomyocytes. This mobility depends on the integrity of both the clathrin-mediated endocytosis pathway and the microtubule network. The channels dynamically oscillate between a mobile/trafficking state and a more static one, determining the protein level expression at the sarcolemma. In permanent AF patients, we observed an increase of  $K_v1.5$  together with a general alteration of markers associated with both retrograde and anterograde trafficking.

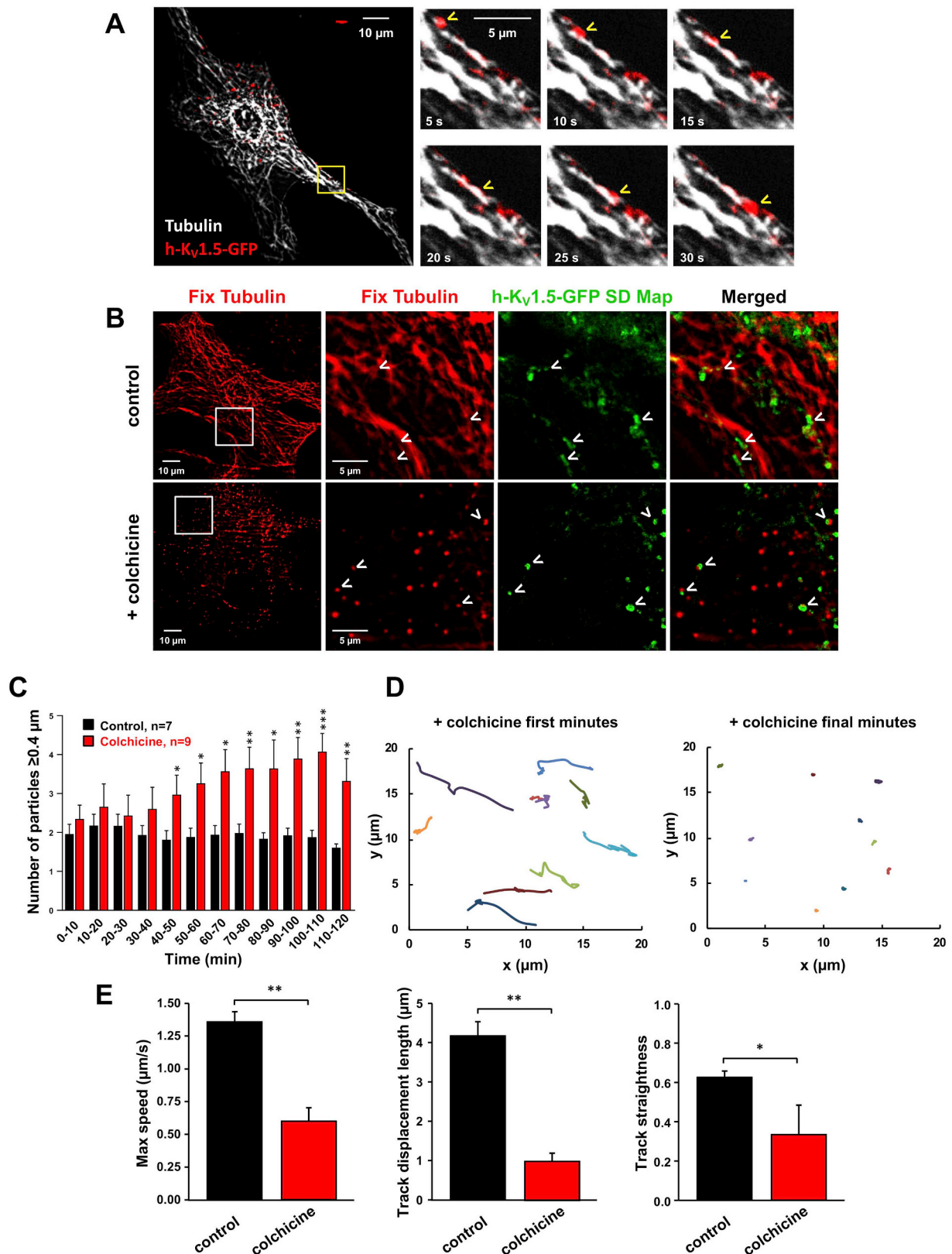
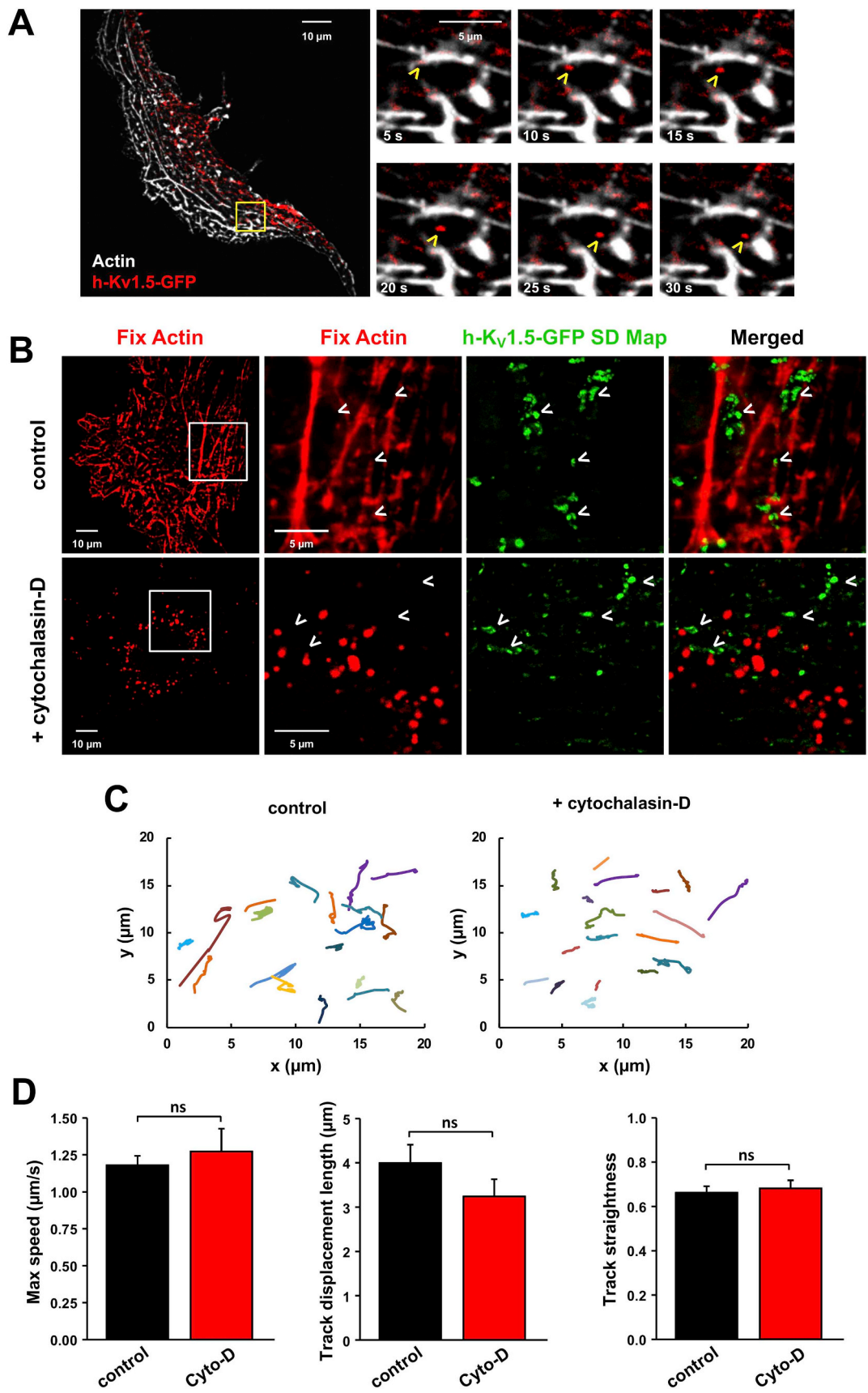


**Fig. 4.** Microtubules disruption reduces K<sub>v</sub>1.5 channel mobility in the sarcolemma of atrial myocytes. **A**, TIRF images of dual color acquisitions from a time series movie showing h-K<sub>v</sub>1.5-GFP particles (red) moving along microtubules (white), and enlargement of one ROI. **B**, Standard deviation maps of h-K<sub>v</sub>1.5-GFP vesicle tracks compared to fixed cell images of microtubules. Arrowheads indicate displacement of h-K<sub>v</sub>1.5-GFP vesicles in control and in colchicine-treated myocytes. **C**, Number of h-K<sub>v</sub>1.5-GFP channel particles over time in control and colchicine conditions. **D**, Tracks generated from TIRF movie illustrating the displacement of h-K<sub>v</sub>1.5-GFP channels in the x/y axis during first (left) and final (right) minutes of colchicine treatment. **E**, Plots of h-K<sub>v</sub>1.5-GFP channel dynamics from fast tracking TIRF movies in control and colchicine conditions. \*P < .05; \*\*P < .01; \*\*\*P < .001; n = 5–15 cells, 50–100 tracks/cell. (For interpretation of the references to color in this figure legend, the reader is referred to the web version of this article.)



(caption on next page)

**Fig. 5.** Actin disruption does not affect  $K_V1.5$  channel mobility in the sarcolemma of atrial myocytes. A, TIRF images of dual color acquisitions from a time series movie showing h- $K_V1.5$ -GFP particles (red) moving between actin (white), and enlargement of one ROI. B, Standard deviation maps of h- $K_V1.5$ -GFP vesicle tracks compared to fixed cell images of actin. Arrowheads indicate displacement of h- $K_V1.5$ -GFP vesicles in control and in cytochalasin-D-treated myocytes. C, Tracks generated from 10 min TIRF movies illustrating the displacement of h- $K_V1.5$ -GFP channels in the x/y axis in control (left) and in cytochalasin-D-treated myocytes (right). D, Plots of h- $K_V1.5$ -EGFP channel dynamics from fast tracking TIRF movies in control and cytochalasin-D conditions. ns, not significant; n = 20–40 cells, 50–100 tracks/cell. (For interpretation of the references to color in this figure legend, the reader is referred to the web version of this article.)

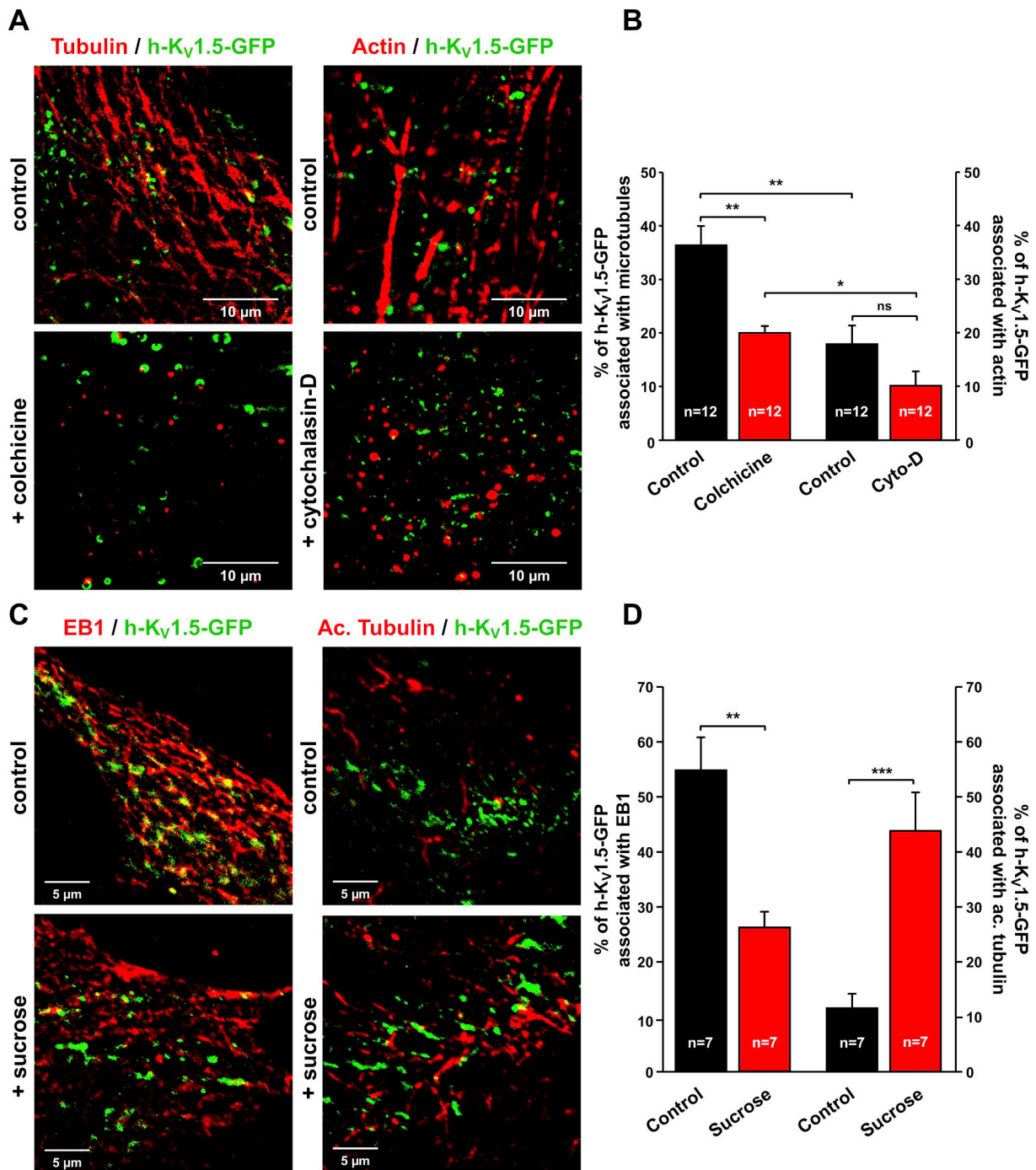
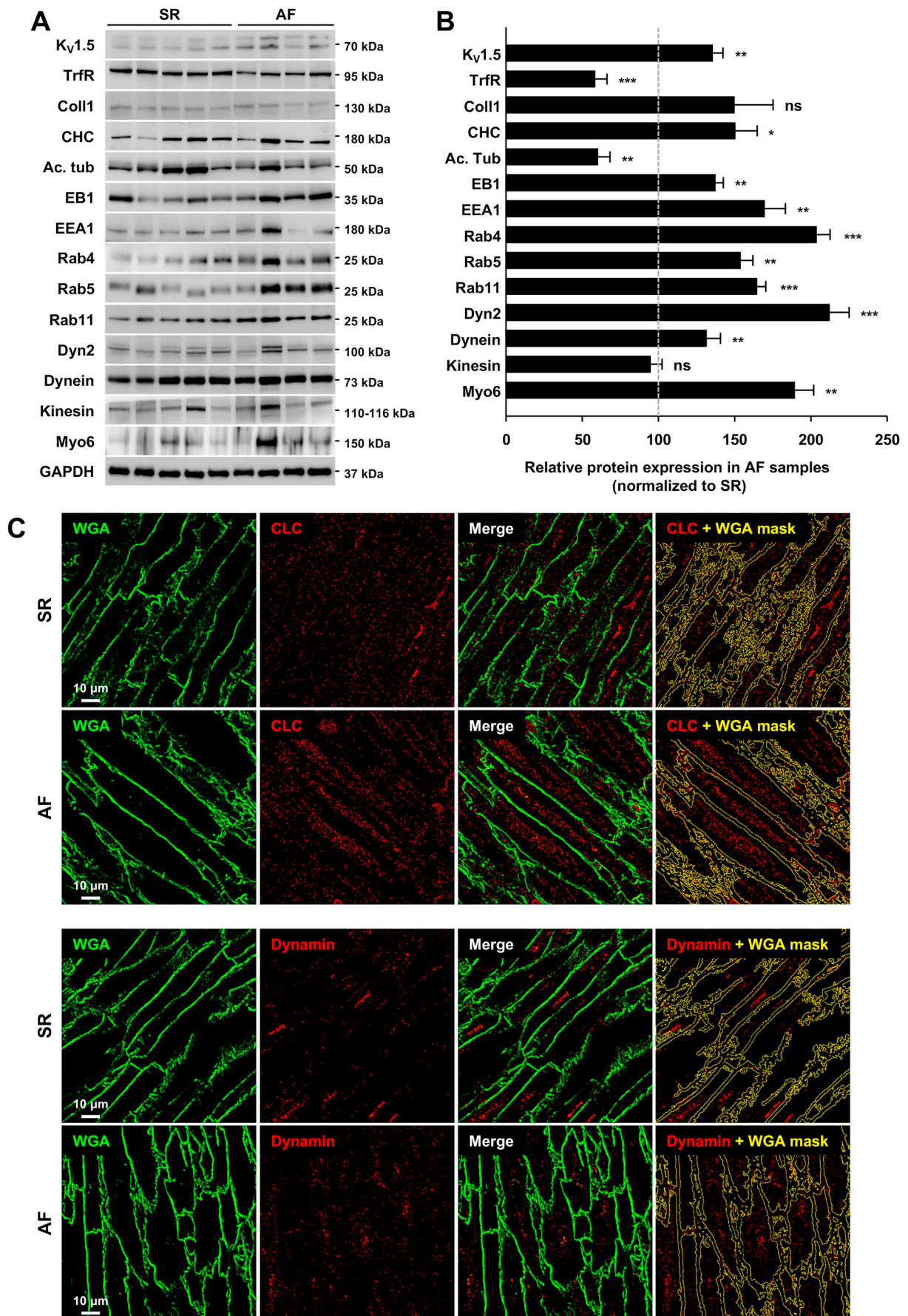


**Fig. 6.** Association of h- $K_V1.5$ -GFP with the cytoskeleton. A, ROIs from images of cultured atrial myocytes expressing h- $K_V1.5$ -GFP and stained with tubulin or actin in control or after treatment with cytoskeleton-disrupting agents colchicine or cytochalasin-D. B, Quantification of association between h- $K_V1.5$ -GFP channels and cytoskeleton markers in control and treated cells. C, ROIs from images of cultured atrial myocytes expressing h- $K_V1.5$ -GFP and stained with dynamic (EB1<sup>+</sup>) or stable (acetylated tubulin<sup>+</sup>) microtubules in control and sucrose conditions. D, Association of h- $K_V1.5$ -GFP vesicles with EB1 or acetylated tubulin in control and sucrose conditions. ns, not significant; \*P < .05; \*\*P < .01; \*\*\*P < .001; n = number of cells.



(caption on next page)

**Fig. 7.** Trafficking-related proteins are altered during atrial fibrillation. A, Representative western blots showing expression levels of  $K_V1.5$ , transferrin receptor, collagen 1 and trafficking-related markers in whole atrial lysates from control (sinus rhythm, SR) and atrial fibrillation patients (AF). B, Quantification of expression levels of proteins normalized to GAPDH and expressed in % changes from SR samples.  $N = 3-10$  experimental replicates;  $n = 4-5$  patients/group. C, Distribution of clathrin light-chain (CLC) and dynamin in SR and AF tissue samples. The membrane marker WGA (left) was used to generate a mask (right) delineating myocyte membranes. D, Distribution of CLC and dynamin signals in the membrane over total fluorescence distribution.  $N = 24-25$  images/patient;  $n = 3$  patients/group. ns, not significant; \* $P < .05$ ; \*\* $P < .01$ ; \*\*\* $P < .001$ .

### 3.1. Clathrin-mediated endocytosis of $K_V1.5$ channel in native atrial myocytes

Previous studies have reported the dynamin-dependent internalization of  $K_V1.5$ , but the precise roles of the clathrin- or caveolin-dependent pathways were not elucidated. Whereas  $K_V1.5$  has been shown to target caveolae in Ltk2 and FRT cells stably expressing  $K_V1.5$  [7,8], a very limited association between  $K_V1.5$  and caveolin-3 has been observed in rat and canine hearts [13]. Using a step sucrose gradient, we previously showed that  $K_V1.5$  and caveolin-3 are found in distinct fractions of proteins extracted from rat atrial myocardium [14]. Our present findings confirm that  $K_V1.5$  channels are not associated with caveolin-3 in atrial myocytes but preferentially associated to clathrin vesicles.

Sucrose is known to induce the formation of clathrin microcages [9], resulting in the observed clusterization and immobilization of  $K_V1.5$  in the membrane plane. Clusterization of  $K_V$  channels in membrane microdomains has been reported for neuronal  $K_V2.1$  channels, which form large immobile clusters locked at the insertion site after delivery to the plasma membrane of hippocampal neurons and transfected HEK cells [15]. Interestingly, clustered  $K_V2.1$  channels do not efficiently conduct  $K^+$ , whereas the non-clustered channels are responsible for the  $K_V2.1$ -mediated current [16]. The fact that sucrose increased track straightness and track displacement length of non-clustered  $K_V1.5$  vesicles suggests an increased persistence of  $K_V1.5$  vesicles in the membrane plane, consistent with a reduction of channel internalization. Our present observation of an increase in  $I_{Kur}$  together with an increased amount of  $K_V1.5$  channel on the membrane surface, clusterization and vesicles persistence in the membrane plane suggests that  $K_V1.5$  channels remains functional after clathrin blockade.

### 3.2. Preferential association of $K_V1.5$ channel with the microtubule network

Alteration of microtubule integrity profoundly affects the surface expression of both potassium and sodium channels. In HEK cells, nocodazole increased both the surface expression of  $K_V1.5$  channels and the  $I_{Kur}$  amplitude [5]. Moreover, colcemid-mediated microtubule disruption impairs the normal surface distribution of  $K_V1.5$  by increasing its internalization in L-cells [7]. Similar results were reported for  $K_V4.2$  and hERG channels. Treatment with dynein inhibitor or overexpression of the p50 protein, which leads to the dissociation of the dynactin/

dynein complex, reproduced the effect of nocodazole-mediated microtubule disruption in HEK cells [17]. In neonatal rat cardiomyocytes, stabilization of the microtubule cytoskeleton reduces  $I_{Na}$  density via a mechanism that reduces channel expression at the sarcolemma [18]. In HL-1 cells, anterograde trafficking of  $K_V1.5$  channel has been shown to occur preferentially on dynamic microtubules associated with the kinesin-2 motor, KIF17 [19]. Microtubules are therefore important determinants of ion channel trafficking in both retrograde and anterograde directions, and here we show how the microtubules network also regulates the dynamics and organization of ion channels within the plasma membrane. Indeed, in control condition  $K_V1.5$  channels were strongly associated with dynamic microtubules ( $EB1^+$ ), while after clathrin blockade they were preferentially associated with stable (acetylated) microtubules. As EB1 indirectly interacts with the dynein/dynactin complex (i.e. microtubule retrograde motor), the fact that microtubules depolymerization mirrored the effect of clathrin blockade strongly suggests a major role of the microtubules network already in the early steps of internalization.

### 3.3. Moderate involvement of the actin cytoskeleton in $K_V1.5$ channel dynamics and internalization

In hippocampal neurons, preventing actin polymerization with latrunculin-A redistributes  $K_V2.1$  channels from cell body to the entire cell, increases clusters size and decreases clusters number, suggesting a role for cortical actin in both clusters maintenance and  $K^+$  channels localization [15]. Manipulating actin cytoskeleton also affects ion channels function by altering their trafficking. In HL-1 cells, for example, cytochalasin-D increases  $K_V1.5$  surface expression [20]. Moreover, both actin depolymerization and  $\alpha$ -actinin2 siRNA increase the  $K_V1.5$ -mediated current and the number of active channels in HEK293 cells. From these observations, it has been suggested that actin cytoskeleton disruption favors the release of intracellularly anchored-pools of channels and their subsequent insertion into the plasma membrane [21]. Similarly, whereas the delivery of connexin-43 at the intercalated disc was shown to be directly mediated by microtubules, actin-associated connexin-43 functions as an alternative trafficking route, providing a cytoplasmic reservoir recruitable in response to cellular stress [10,22]. Here, disruption of the actin cytoskeleton affected retrograde trafficking to similar extent to that of microtubule disruption, but only slightly affected anterograde trafficking and did not change  $K_V1.5$  dynamics in the membrane plane. Since an indirect linkage to the actin cytoskeleton via  $\alpha$ -actinin2 have been reported for  $K_V1.5$  [21], one could hypothesize that the decrease in detectable moving particles after cytochalasin-D treatment affects a binding protein that participates in the labile/transitory maintenance of  $K_V1.5$  channel in the membrane plane. Taken together these results indicate that the actin cytoskeleton has a limited role in  $K_V1.5$  channel anterograde trafficking and membrane organization in atrial myocytes, supporting our previous observation that  $K_V1.5$  channel delivery to the sarcolemma relies more on the microtubule network rather than on cortical actin cytoskeleton [4].

### 3.4. Physiological relevance during permanent atrial fibrillation

Changes in channel expression are now recognized as the main mechanism underlying the altered electrical properties of diseased myocardium. Furthermore, during AF,  $K_V1.5$  channel expression varies with arrhythmia duration, as indicated by the observation of a positive

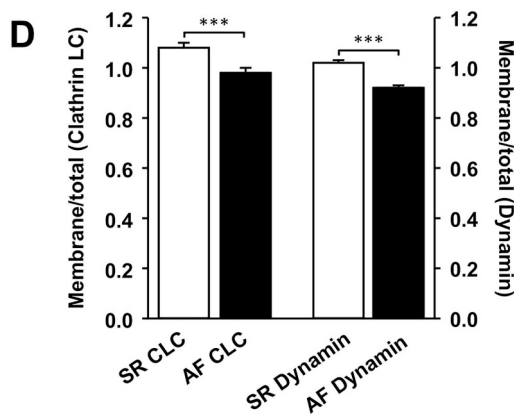


Fig. 7. (continued)

correlation between channel protein density and the duration of the sinus rhythm after the last paroxysmal AF episode [23]. Similarly, a fast and transient increase in  $K_v1.5$  channel expression has been observed during paroxysmal atrial tachycardia in rats [24]. Moreover, we previously reported that chronic hemodynamic overload of the atria, an AF risk factor, stimulates  $K_v1.5$  channel recycling and exocytosis [4]. The present study suggests that  $K_v1.5$  channel dynamics also contribute to the complex pattern of  $K_v1.5$  channel expression during disease progression. Our findings of up-regulated recycling pathways and reduced clathrin-mediated endocytosis are consistent with an accumulation of  $K_v1.5$  channels in the sarcolemma of atrial myocytes from patients in permanent AF. Altogether, these observations fit the AF model based on the shortening of the APD and ERP as substrate for re-entry wavelets in the atria [25]. In support of this model for AF,  $K_v1.5$  gain-of-function mutations have been identified in patients with early-onset lone AF [26]. Moreover, the induction and maintenance of AF through the shortening of the ERP has been confirmed in animal models [27–29], mathematical models [30], and reports of AF induced by gain-of-function mutations in other cardiac potassium channels including  $KCNQ1/KCNE1-2$  and  $KCNJ2$  [31–33],  $Kir2.1$  [34], and  $hERG$  [35]. Finally, alteration of the microtubule network state, as observed in remodeled atrial myocytes, could also impact  $K_v1.5$  channel properties; but further studies are needed to fully elucidate the role of microtubules. Nevertheless, the machinery identified in this study provides mechanistic insight into how  $K_v1.5$  dynamics play a major role in the adaptation of atrial electrical properties to modifications of mechanical and/or homeostatic states of the atrial myocardium, whether in physiological or pathological settings [3,4,11].

#### 4. Materials and methods

An extensive Material and Methods section is available in the Online Data Supplement.

##### 4.1. Cell preparation, adenoviral infections

Adult rat atrial myocytes were obtained by enzymatic dissociation on a Langendorff column as previously described [4]. Atrial myocytes were transduced 24 h after isolation with Ad-human(h)- $K_v1.5$ -EGFP, Ad-human(h)- $K_v1.5$ -HA, or transfected with siRNA (si-clathrin heavy-chain). Actin filaments and microtubules were live stained with RFP fluorescent dyes (CellLight®, ThermoFisher). All studies were performed between 3 and 4 days post-transduction or transfection.

##### 4.2. Electrophysiological measurements

Patch-clamp recordings were performed in the whole-cell configuration at room temperature. Detailed solutions and protocols are available in the Online Data Supplement.

##### 4.3. Deconvolution microscopy and image analysis

Epifluorescence imaging was performed using a Plan APO 60× Oil, 1.42 NA objective in an Olympus IX-71 microscope. Digital images were captured in the Z-axis in 0.2  $\mu\text{m}$  increments. Images were deconvoluted using acquired PSF with DeltaVision Elite microscopy system (GE Healthcare). Fluorescence quantification and colocalization analysis were performed using ImageJ (NIH) or Imaris 8/9 (Bitplane) softwares. Stacks of 4  $\mu\text{m}$ -thick were used for perspectives views/volume rendering, otherwise 3 consecutive stacks were used for image analysis.

##### 4.4. Evanescent field microscopy, vesicle tracking and dynamic parameters

Cells were visualized with total internal reflection fluorescence (TIRF) microscopy using the Olympus Cell<sup>TIRF</sup> system as previously described [4]. Vesicle tracking was performed using ImarisTrack. Time

series of 360 images at 20s intervals were acquired for control, sucrose and colchicine movies; time series of 150 images at 5 s intervals were acquired for control and cytochalasin-D movies. For measurements of single particles dynamics, time series of 240 images every 0.5 s were acquired for all the conditions listed above.

##### 4.5. Generation of SD maps from images series

Standard Deviation (SD) images were constructed from image stacks containing 30 images corresponding to a time series of 600 s using the Z-projection/StandardDeviation plugin of ImageJ. The SD map representing the variation in fluorescence intensity for each pixel location in the raw images was used to highlight the h- $K_v1.5$ -GFP mobility and was overlapped with average fluorescence images (fixed: Z-projection/Average) of cytoskeleton.

##### 4.6. Human samples

In accordance with approval of Institution Ethic Committee, biopsies of right atrial appendages were obtained from patients undergoing cardiac surgery. See Online Data Supplement.

##### 4.7. Statistics

Data are represented as mean  $\pm$  SEM; \*:  $P < .05$ , \*\*:  $P < .01$  and \*\*\*:  $P < .001$ ; ns: not significant.

Supplementary data to this article can be found online at <https://doi.org/10.1016/j.yjmcc.2020.05.004>.

##### Source of funding

This work was supported by the European Union (EUTRAF-261057; EB and SH) and the Fondation pour la Recherche Médicale (FRM-DEQ20160334880; EB and SH).

##### Declaration of Competing Interest

None.

##### Acknowledgments

We thank Dr. C. Longin, MIMA2-UMR1131 GABI, Plateau de Microscopie Electronique, Jouy-en-Josas, France for her help with electron microscopy acquisitions.

##### References

- [1] M. Furutani, M.C. Trudeau, N. Hagiwara, A. Seki, Q. Gong, Z. Zhou, et al., Novel mechanism associated with an inherited cardiac arrhythmia: defective protein trafficking by the mutant  $HERG$  (G601S) potassium channel, *Circulation* 99 (17) (4 May 1999) 2290–2294.
- [2] J. Guo, H. Massaeli, J. Xu, Z. Jia, J.T. Wigle, N. Mesaali, et al., Extracellular  $K^+$  concentration controls cell surface density of  $I_{Kr}$  in rabbit hearts and of the  $HERG$  channel in human cell lines, *J. Clin. Invest.* 119 (9) (Sep 2009) 2745–2757.
- [3] E. Balse, S. El-Haou, G. Dillanian, A. Dauphin, J. Eldstrom, D. Fedida, et al., Cholesterol modulates the recruitment of  $K_v1.5$  channels from Rab11-associated recycling endosome in native atrial myocytes, *Proc. Natl. Acad. Sci. U. S. A.* 106 (34) (25 Aug 2009) 14681–14686.
- [4] H.E. Boycott, C.S.M. Barbier, C.A. Eichel, K.D. Costa, R.P. Martins, F. Louault, et al., Shear stress triggers insertion of voltage-gated potassium channels from intracellular compartments in atrial myocytes, *Proc. Natl. Acad. Sci. U. S. A.* 110 (41) (8 Oct 2013) E3955–E3964.
- [5] W.S. Choi, A. Khurana, R. Mathur, V. Viswanathan, D.F. Steele, D. Fedida,  $K_v1.5$  surface expression is modulated by retrograde trafficking of newly endocytosed channels by the dynein motor, *Circ. Res.* 97 (4) (19 Aug 2005) 363–371.
- [6] McEwen DP, S.M. Schumacher, Q. Li, M.D. Benson, J.A. Iñiguez-Lluhí, K.M. Van Genderen, et al., Rab-GTPase-dependent endocytic recycling of  $K_v1.5$  in atrial myocytes, *J. Biol. Chem.* 282 (40) (5 Oct 2007) 29612–29620.
- [7] J.R. Martens, N. Sakamoto, S.A. Sullivan, T.D. Grobaski, M.M. Tamkun, Isoform-specific localization of voltage-gated  $K^+$  channels to distinct lipid raft populations. Targeting of  $K_v1.5$  to caveolae, *J. Biol. Chem.* 276 (11) (16 Mar 2001) 8409–8414.

- [8] D.P. McEwen, Q. Li, S. Jackson, P.M. Jenkins, J.R. Martens, Caveolin regulates kv1.5 trafficking to cholesterol-rich membrane microdomains, *Mol. Pharmacol.* 73 (3) (Mar 2008) 678–685.
- [9] J.E. Heuser, R.G. Anderson, Hypertonic media inhibit receptor-mediated endocytosis by blocking clathrin-coated pit formation, *J. Cell Biol.* 108 (2) (Feb 1989) 389–400.
- [10] J.W. Smyth, J.M. Vogan, P.J. Buch, S.-S. Zhang, T.S. Fong, T.-T. Hong, et al., Actin cytoskeleton rest stops regulate anterograde traffic of connexin 43 vesicles to the plasma membrane, *Circ. Res.* 110 (7) (30 Mar 2012) 978–989.
- [11] E. Balse, D.F. Steele, H. Abriel, A. Coulombe, D. Fedida, S.N. Hatem, Dynamic of ion channel expression at the plasma membrane of cardiomyocytes, *Physiol. Rev.* 92 (3) (Jul 2012) 1317–1358.
- [12] A.D. Zadeh, H. Xu, M.E. Loewen, G.P. Noble, D.F. Steele, D. Fedida, Internalized Kv1.5 traffics via Rab-dependent pathways, *J. Physiol.* 586 (20) (15 Oct 2008) 4793–4813.
- [13] J. Eldstrom, D.R. Van Wagoner, E.D. Moore, D. Fedida, Localization of Kv1.5 channels in rat and canine myocyte sarcolemma, *FEBS Lett.* 580 (26) (13 Nov 2006) 6039–6046.
- [14] J. Abi-Char, A. Maguy, A. Coulombe, E. Balse, P. Ratajczak, J.-L. Samuel, et al., Membrane cholesterol modulates Kv1.5 potassium channel distribution and function in rat cardiomyocytes, *J. Physiol.* 582 (Pt 3) (1 Aug 2007) 1205–1217.
- [15] K.M.S. O'Connell, A.S. Rolig, J.D. Whitesell, M.M. Tamkun, Kv2.1 potassium channels are retained within dynamic cell surface microdomains that are defined by a perimeter fence, *J. Neurosci.* 26 (38) (20 Sep 2006) 9609–9618.
- [16] K.M.S. O'Connell, R. Loftus, M.M. Tamkun, Localization-dependent activity of the Kv2.1 delayed-rectifier K<sup>+</sup> channel, *Proc. Natl. Acad. Sci. U. S. A.* 107 (27) (6 Jul 2010) 12351–12356.
- [17] M.E. Loewen, Z. Wang, J. Eldstrom, A. Dehghani Zadeh, A. Khurana, D.F. Steele, et al., Shared requirement for dynein function and intact microtubule cytoskeleton for normal surface expression of cardiac potassium channels, *Am. J. Physiol. Heart Circ. Physiol.* 296 (1) (2009) H71–H83.
- [18] S. Casini, H.L. Tan, I. Demirayak, C.A. Remme, A.S. Amin, B.P. Scicluna, et al., Tubulin polymerization modifies cardiac sodium channel expression and gating, *Cardiovasc. Res.* 85 (4) (1 Mar 2010) 691–700.
- [19] D. Cai, D.P. McEwen, J.R. Martens, E. Meyhofer, K.J. Verhey, Single molecule imaging reveals differences in microtubule track selection between kinesin motors, *PLoS Biol.* 7 (10) (Oct 2009) e1000216.
- [20] S.M. Schumacher-Bass, E.D. Vesely, L. Zhang, K.E. Ryland, D.P. McEwen, P.J. Chan, et al., Role for myosin-V motor proteins in the selective delivery of Kv channel isoforms to the membrane surface of cardiac myocytes, *Circ. Res.* 114 (6) (14 Mar 2014) 982–992.
- [21] N.D. Maruoka, D.F. Steele, B.P. Au, P. Dan, X. Zhang, E.D. Moore, et al., alpha-actinin-2 couples to cardiac Kv1.5 channels, regulating current density and channel localization in HEK cells, *FEBS Lett.* 473 (2) (12 May 2000) 188–194.
- [22] R.M. Shaw, A.J. Fay, M.A. Puthenveedu, M. von Zastrow, Y.-N. Jan, L.Y. Jan, Microtubule plus-end-tracking proteins target gap junctions directly from the cell interior to adherens junctions, *Cell* 128 (3) (9 Feb 2007) 547–560.
- [23] B.J. Brundel, I.C. Van Gelder, R.H. Henning, A.E. Tuinenburg, M. Wietses, J.G. Grandjean, et al., Alterations in potassium channel gene expression in atria of patients with persistent and paroxysmal atrial fibrillation: differential regulation of protein and mRNA levels for K<sup>+</sup> channels, *J. Am. Coll. Cardiol.* 37 (3) (1 Mar 2001) 926–932.
- [24] T. Yamashita, Y. Murakawa, N. Hayami, E.I. Fukui, Y. Kasaoka, M. Inoue, et al., Short-term effects of rapid pacing on mRNA level of voltage-dependent K(+) channels in rat atrium: electrical remodeling in paroxysmal atrial tachycardia, *Circulation* 101 (16) (25 Apr 2000) 2007–2014.
- [25] S. Nattel, New ideas about atrial fibrillation 50 years on, *Nature* 415 (6868) (Jan 2002) 219–226.
- [26] I.E. Christophersen, M.S. Olesen, B. Liang, M.N. Andersen, A.P. Larsen, J.B. Nielsen, et al., Genetic variation in KCNA5: impact on the atrial-specific potassium current IKur in patients with lone atrial fibrillation, *Eur. Heart J.* 34 (20) (May 2013) 1517–1525.
- [27] D.R. Van Wagoner, Electrophysiological remodeling in human atrial fibrillation, *Pacing Clin. Electrophysiol.* PACE 26 (7 Pt 2) (Jul 2003) 1572–1575.
- [28] M.C. Wijffels, C.J. Kirchhof, R. Dorland, M.A. Allesie, Atrial fibrillation begets atrial fibrillation. A study in awake chronically instrumented goats, *Circulation* 92 (7) (1 Oct 1995) 1954–1968.
- [29] L. Geng, S. Wang, F. Zhang, K. Xiong, J. Huang, T. Zhao, et al., SNX17 (sorting nexin 17) mediates atrial fibrillation onset through endocytic trafficking of the Kv1.5 (potassium voltage-gated channel subfamily a member 5) channel, *Circ. Arrhythm. Electrophysiol.* 12 (4) (2019) e007097.
- [30] S.V. Pandit, O. Berenfeld, J.M.B. Anumonwo, R.M. Zariwsky, J. Kneller, S. Nattel, et al., Ionic determinants of functional reentry in a 2-D model of human atrial cells during simulated chronic atrial fibrillation, *Biophys. J.* 88 (6) (Jun 2005) 3806–3821.
- [31] S. Mahida, S.A. Lubitz, M. Rienstra, D.J. Milan, P.T. Ellinor, Monogenic atrial fibrillation as pathophysiological paradigms, *Cardiovasc. Res.* 89 (4) (1 Mar 2011) 692–700.
- [32] Y.-H. Chen, S.-J. Xu, S. Bendahhou, X.-L. Wang, Y. Wang, W.-Y. Xu, et al., KCNQ1 gain-of-function mutation in familial atrial fibrillation, *Science* 299 (5604) (10 Jan 2003) 251–254.
- [33] Y. Yang, M. Xia, Q. Jin, S. Bendahhou, J. Shi, Y. Chen, et al., Identification of a KCNE2 gain-of-function mutation in patients with familial atrial fibrillation, *Am. J. Hum. Genet.* 75 (5) (Nov 2004) 899–905.
- [34] M. Xia, Q. Jin, S. Bendahhou, Y. He, M.-M. Larroque, Y. Chen, et al., A Kir2.1 gain-of-function mutation underlies familial atrial fibrillation, *Biochem. Biophys. Res. Commun.* 332 (4) (15 Jul 2005) 1012–1019.
- [35] K. Hong, P. Bjerregaard, I. Gussak, R. Brugada, Short QT syndrome and atrial fibrillation caused by mutation in KCNH2, *J. Cardiovasc. Electrophysiol.* 16 (4) (Apr 2005) 394–396.